 CMES, vol.113, no.3, pp.343-366, 2017

Axisymmetric Slow Motion of a Prolate Particle in a Circular Capillary with Slip Surfaces

Hong Y. Yeh, Huan J. Keh[1]*

Abstract: The problem of the steady migration of an axially symmetric prolate particle along its axis of revolution coinciding with the centerline of a circular capillary is investigated semi-analytically in the limit of low Reynolds number, where the viscous fluid may slip at the solid surfaces. A method of distribution of spherical singularities along the axis inside the particle is employed to establish the general solution of the fluid velocity satisfying the boundary conditions at the capillary wall and infinity. The slip condition at the particle surface is then satisfied by using a boundary collocation method to determine the unknown constants in this solution. The hydrodynamic drag force acting on the particle is obtained with good convergence for the cases of a prolate spheroid and a prolate Cassini oval with various values of the slip parameter of the particle, slip parameter of the capillary wall, aspect ratio or shape parameter of the particle, and spacing parameter between the particle and the wall. For the axially symmetric migrations of a spheroid and a Cassini oval in a capillary with no-slip surfaces and of a sphere in a capillary with slip surfaces, our results agree excellently with the numerical solutions obtained earlier. The capillary wall affects the particle migration significantly when the solid surfaces get close to each other. For a specified particle-in-capillary configuration, the normalized drag force exerted on the particle in general decreases with increasing slippage at the solid surfaces, except when the fluid slips little at the capillary wall and the particle-wall spacing parameter is relatively large. For fixed spacing parameter and slip parameters, the drag force increases with an increase in the axial-to-radial aspect ratio (or surface area effective for viscous interaction with the capillary wall) of the particle, but this tendency can be reversed when the particle is highly slippery.

Keywords: Creeping flow, prolate spheroid, passini oval, Navier's slip, singularity distribution, boundary collocation.

1 Introduction

The creeping motions of small particles in viscous fluids are of much fundamental and practical interest in many areas of science and technology. The theoretical treatment of this subject grew out of the classic work of Stokes (1851) for a no-slip spherical particle

[1] Department of Chemical Engineering, National Taiwan University, Taipei, 10617, Taiwan, ROC.

*Corresponding author: E-mail: huan@ntu.edu.tw.

migrating in an unbounded, incompressible, Newtonian fluid. Oberbeck (1876) extended this analysis to the migration of an ellipsoid. More recently, analytical results of low-Reynolds-number motions were obtained for a particle whose boundary conforms to a coordinate surface of one orthogonal curvilinear coordinate system in which the Stokes equations are simply separable [Payne and Pell (1960)] or semi-separable [Dassios, Hadjinicolaou, and Payatakes (1994)], for a slightly deformed sphere [Brenner (1964)], and for a slender body [Batchelor (1970)]. Additionally, the creeping motions of a particle of specific or general shape have been investigated semi-analytically by using the boundary collocation method [Gluckman, Pfeffer, and Weinbaum (1971)], boundary integral method [Youngren and Acrivos (1975)], and singularity method [Chwang and Wu (1975)].

When one tries to solve the creeping-flow problems, no-slip boundary conditions are usually taken at the solid-fluid interfaces. Although this assumption is validated by experimental evidences at macroscopic scales, it is seldom accepted microscopically [Pit, Hervet and Leger (2000); Martini et al. (2008)]. The phenomena that the adjacent fluid slips frictionally over a solid surface occur in many cases, such as the rarefied gas flow past an aerosol particle [Ying and Peters (1991); Keh and Shiau (2000)], liquid flow next to a lyophobic surface [Churaev, Sobolev, and Somov (1984); Gogte et al. (2005)], micropolar fluid flow around a rigid particle [Sherif, Faltas, and Saad (2008)], and viscous fluid flow over the surface of a porous medium [Saffman (1971); Nir (1976)] or a small particle of molecular size [Hu and Zwanzig (1974)]. Presumably, any such slipping would be proportional to the local shear stress of the fluid adjacent to the solid surface [Felderhof (1977); Keh and Chen (1996)], known as Navier’s slip [Eqs. (4) and (5)], and the proportionality constant β^{-1} is termed the slip coefficient of the solid-fluid interface.

The drag force acting on a migrating spherical particle of radius b with a slip surface by an unbounded fluid of viscosity η can be expressed as [Basset (1961); Happel and Brenner (1983)]

$$F = -6\pi\eta b U \frac{\beta b + 2\eta}{\beta b + 3\eta}, \tag{1}$$

where U is the velocity of the particle. The practical values of the dimensionless parameter $\beta b/\eta$ are greater than about 10 for aerosol systems with the Knudsen number smaller than 0.1, but can be much less for other systems involving frictional slip such as the water flow around a particle with hydrophobic surface. When $\beta b/\eta \to \infty$, there is no slip at the particle surface and Eq. (1) becomes Stokes’ law. When $\beta b/\eta = 0$, there is a perfect slip and the particle acts like a gas bubble sphere with $F = -4\pi\eta b U$.

The analysis of creeping motion of a no-slip particle which deforms slightly in shape from a sphere in an arbitrary direction pioneered by Brenner (1964) was extended to a slightly deformed slip sphere and closed-form expressions for the hydrodynamic drag force exerted on it were obtained to the first order [Palaniappan (1994); Senchenko and Keh (2006)] and second order [Chang and Keh (2009)] in the small parameter characterizing the deformation. On the other hand, the semi-separable general solution in the form of an infinite series expansion for the axisymmetric creeping flow in spheroidal coordinates developed by Dassios, Hadjinicolaou, and Payatakes (1994) was used to examine the slip flow past a spheroid and to derive the drag force experienced by it in explicit forms [Deo and Datta (2002); Keh and Chang (2008)]. Recently, the creeping flows caused by a general axisymmetric particle with a slip surface migrating parallel [Keh and Huang (2004); Wan and Keh (2009)] and perpendicular [Chang and Keh (2011)] to its axis of revolution have been studied semi-analytically by using a method of internal singularity distribution incorporated with a boundary collocation technique.

In real situations of colloidal motion, particles are seldom isolated and will move in the presence of confining boundaries. Therefore, the boundary effects on creeping motion of particles with fluid slip at the solid surfaces are essential and have been investigated for various cases of a confined sphere [Reed and Morrison (1974); Chen and Keh (1995); Keh and Chang (1998); Lu and Lee (2002); Chen and Keh (2003); Chang and Keh (2006); Keh and Chang (2007); Keh and Lee (2010); Faltas and Saad (2011); Lee and Keh (2013, 2014); Chiu and Keh (2016, 2017); Li and Keh (2017)]. Recently, the axisymmetric translation [Keh and Chang (2010)] and rotation [Wan and Keh (2011)] of a slip particle of revolution at an arbitrary position between two parallel plane walls have also been studied using the method of distributed internal singularities. In the current article, we adopt the same method to analyze the creeping flow caused by a general prolate particle of revolution undergoing axially symmetric migration in a circular capillary with slip surfaces. The drag forces acting on a spheroid and a Cassini oval (which has various configurations from a sphere to a partially concave body as its shape parameter takes different values) by the suspending fluid are numerically calculated with good convergence for broad ranges of the particle shape parameter, particle-to-capillary size ratio, and normalized slip coefficients. These results agree excellently with those available in the literature for the particular cases of a slip sphere, a no-slip spheroid, and a no-slip Cassini oval migrating in the capillary.

2 Mathematical formulation of the general problem

Consider the steady creeping motion of an axially symmetric, prolate particle along its axis of revolution which is also the centerline of a circular capillary of radius R filled with a quiescent, incompressible, Newtonian fluid of viscosity η, as shown in Fig.1. Here (ρ, ϕ, z) and (r, θ, ϕ) are the circular cylindrical and spherical coordinate systems, respectively, with the origin at the center of the particle. The particle migrates with a velocity $U\mathbf{e}_z$, where $\mathbf{e}_z$ is the unit vector in the z direction. The fluid may slip frictionally at the particle surface S_p and at the capillary wall $\rho = R$.

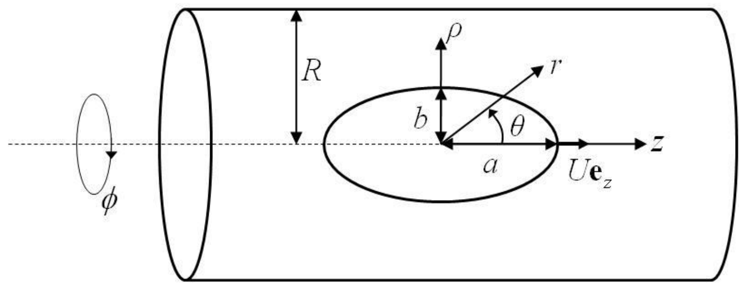

Figure 1: Geometrical sketch for the migration of an axisymmetric prolate particle along its axis of revolution in a coaxial circular capillary.

The Reynolds number is sufficiently small so that the fluid motion is governed by the Stokes equations,

$$\eta\nabla^2\mathbf{v} - \nabla p = \mathbf{0}, \tag{2}$$

$$\nabla\cdot\mathbf{v} = 0, \tag{3}$$

where $\mathbf{v}$ and p are the fluid velocity field and dynamic pressure distribution, respectively. The boundary conditions at the particle surface, at the capillary wall, and far from the particle are

$$\mathbf{v} = U\mathbf{e}_z + \frac{1}{\beta}(\mathbf{I}-\mathbf{nn})\mathbf{n}:\boldsymbol{\tau} \quad \text{on } \mathrm{S_p}, \tag{4}$$

$$\mathbf{v} = -\frac{1}{\beta_\mathrm{w}}(\mathbf{I}-\mathbf{e}_\rho\mathbf{e}_\rho)\mathbf{e}_\rho:\boldsymbol{\tau} \quad \text{at } \rho = R, \tag{5}$$

$$\mathbf{v}\to\mathbf{0} \qquad \text{as } |z|\to\infty. \tag{6}$$

Here, $\boldsymbol{\tau} = \eta[\nabla\mathbf{v} + (\nabla\mathbf{v})^\mathrm{T}]$ is the viscous stress tensor, $\mathbf{e}_\rho$ is the unit vector in the ρ direction, $\mathbf{n}$ is the unit normal vector on the particle surface S_p pointing into the fluid, $\mathbf{I}$ is the unit dyadic, and the constants $1/\beta$ and $1/\beta_\mathrm{w}$ are the Navier slip coefficients about the particle surface and capillary wall, respectively.

To solve Eqs. (2) - (6) for the axially symmetric motion, a set of spherical singularities satisfying Eqs. (2), (3), (5), and (6) will be distributed along the axis of revolution inside the particle. The fluid flow field is constructed by the superposition of these singularities and the boundary condition (4) over the particle surface can be satisfied by using a multipole collocation method.

The fluid velocity components in circular cylindrical coordinates caused by a spherical singularity at the point $\rho = 0$ and $z = h$ are [Keh and Chang (2007)]

$$v_\rho = \sum_{n=2}^{\infty}[B_n A_{1n}(\rho,z,h) + D_n A_{2n}(\rho,z,h)], \tag{7}$$

$$v_z = \sum_{n=2}^{\infty} [B_n C_{1n}(\rho, z, h) + D_n C_{2n}(\rho, z, h)], \tag{8}$$

and $v_\phi = 0$, where A_{in} and C_{in} with $i = 1$ and 2 are functions defined by Eqs. (A1) and (A2) in Appendix A, and B_n and D_n are unknown constants. The hydrodynamic drag force acting on the particle due to this singularity is related to the constant D_2 by

$$F = 4\pi\eta D_2 . \tag{9}$$

A segment along the axis of revolution ($\rho = 0$) between the points $z = c_1 \le 0$ and $z = c_2 \ge 0$ within the particle is taken on which a set of spherical singularities are distributed. The general solution of the fluid velocity can be approximated by the superposition of these singularities into the integral form of Eqs. (7) and (8),

$$\begin{bmatrix} v_\rho \\ v_z \end{bmatrix} = \sum_{n=2}^{\infty} \int_{c_1}^{c_2} \{ B_n(t) \begin{bmatrix} A_{1n}(\rho, z, t) \\ C_{1n}(\rho, z, t) \end{bmatrix} + D_n(t) \begin{bmatrix} A_{2n}(\rho, z, t) \\ C_{2n}(\rho, z, t) \end{bmatrix} \} \mathrm{d}t , \tag{10}$$

where $B_n(t)$ and $D_n(t)$ are the unknown density distribution functions.

In order to use the boundary collocation method, we apply the *M*-point Gauss-Legendre quadrature of integration [Hornbeck (1975)] to Eq. (10) and truncate the infinite series after N terms to result in

$$\begin{bmatrix} v_\rho \\ v_z \end{bmatrix} = \sum_{n=2}^{N+1} \sum_{m=1}^{M} \{ B_{nm} \begin{bmatrix} A_{1n}(\rho, z, q_m) \\ C_{1n}(\rho, z, q_m) \end{bmatrix} + D_{nm} \begin{bmatrix} A_{2n}(\rho, z, q_m) \\ C_{2n}(\rho, z, q_m) \end{bmatrix} \} , \tag{11}$$

where q_m are the quadrature zeros, and the unknown density constants B_{nm} and D_{nm} need to be determined from the boundary condition (4) at the particle surface. From Eq. (11) for the fluid velocity, the non-vanishing components of the symmetric viscous stress tensor in Eqs. (4) and (5) in cylindrical coordinates are obtained as

$$\begin{bmatrix} \tau_{\rho\rho} \\ \tau_{zz} \\ \tau_{\rho z} \end{bmatrix} = \eta \sum_{n=2}^{N+1} \sum_{m=1}^{M} \{ B_{nm} \begin{bmatrix} \alpha_{1n}(\rho, z, q_m) \\ \beta_{1n}(\rho, z, q_m) \\ \gamma_{1n}(\rho, z, q_m) \end{bmatrix} + D_{nm} \begin{bmatrix} \alpha_{2n}(\rho, z, q_m) \\ \beta_{2n}(\rho, z, q_m) \\ \gamma_{2n}(\rho, z, q_m) \end{bmatrix} \} , \tag{12}$$

where the functions α_{in}, β_{in}, and γ_{in} are defined by Eqs. (A3) - (A5).

Substituting Eqs. (11) and (12) into Eq. (4), we obtain

$$\sum_{n=2}^{N+1} \sum_{m=1}^{M} \{ B_{nm} \begin{bmatrix} A^*_{1n}(\rho, z, q_m) \\ C^*_{1n}(\rho, z, q_m) \end{bmatrix} + D_{nm} \begin{bmatrix} A^*_{2n}(\rho, z, q_m) \\ C^*_{2n}(\rho, z, q_m) \end{bmatrix} \} = \begin{bmatrix} 0 \\ U \end{bmatrix} \qquad \text{on} \quad S_\mathrm{p} , \tag{13}$$

where

$$A_{in}^{*}(\rho,z,h)=A_{in}(\rho,z,h)-\frac{\eta}{\beta}[(1-n_{\rho}^{2})n_{\rho}\alpha_{in}(\rho,z,h)-n_{\rho}n_{z}^{2}\beta_{in}(\rho,z,h)$$
$$+(1-2n_{\rho}^{2})n_{z}\gamma_{in}(\rho,z,h)], \tag{14}$$
$$C_{in}^{*}(\rho,z,h)=C_{in}(\rho,z,h)-\frac{\eta}{\beta}[(1-n_{z}^{2})n_{z}\beta_{in}(\rho,z,h)-n_{z}n_{\rho}^{2}\alpha_{in}(\rho,z,h)$$
$$+(1-2n_{z}^{2})n_{\rho}\gamma_{in}(\rho,z,h)], \tag{15}$$

and n_ρ and n_z are the local ρ and z components, respectively, of the unit normal $\mathbf{n}$. The boundary collocation method allows Eq. (13) to be satisfied at MN values of θ ($0\le\theta\le\pi$) on the particle surface and results in a set of $2MN$ simultaneous linear algebraic equations, which can be solved numerically to yield the $2MN$ density constants B_{nm} and D_{nm} required in Eq. (11) for the fluid velocity components. The accuracy of the collocation method can be improved to a satisfactory degree by taking sufficiently large values of M and N. Once the constants D_{2m} are determined, the hydrodynamic drag force acting on the particle can be obtained from Eq. (9) as

$$F=4\pi\eta\sum_{m=1}^{M}D_{2m}\,. \tag{16}$$

In the next two sections, the above-described semi-analytical procedure will be taken to solve for the axisymmetric motions of a prolate spheroid and a prolate Cassini oval, respectively, in a circular capillary. In both cases, the streamline geometry is symmetric about z and only the terms with even n are retained in Eqs. (11) - (13). For the simple case of migration of a spherical particle (can be degenerated from either spheroid or Cassini oval) along the axis of the circular capillary with slip surfaces, only one singularity at the particle center (with $h=0$) is needed and the numerical results of the drag force have been obtained by Keh and Chang (2007).

3 Motion of a prolate spheroid

In this section, we consider the migration of a prolate spheroid along its axis of revolution in a coaxial circular capillary, where the fluid is allowed to slip at the solid surfaces. The surface of a prolate spheroid and the local components of its unit normal in Eqs. (14) and (15) are given by

$$\rho=b[1-(\frac{z}{a})^{2}]^{1/2}, \tag{17}$$

and

$$n_{\rho}=\frac{(a/b)^{2}\rho}{\sqrt{(a/b)^{4}\rho^{2}+z^{2}}},\qquad n_{z}=\frac{z}{\sqrt{(a/b)^{4}\rho^{2}+z^{2}}}, \tag{18}$$

where a and b are the major and minor semi-axes, respectively. For the axially symmetric migration of a slip prolate spheroid in an unbounded fluid, analytical and numerical results of the hydrodynamic drag force F_0 are available in the literature [Keh and Huang (2004); Keh and Chang (2008); Chang and Keh (2009)].

The method of combined singularity distribution and boundary collocation presented in the previous section is used to obtain the solution for the axisymmetric migration of a prolate spheroid in a circular capillary with slip surfaces. The details of the numerical scheme used for this work were given in an earlier paper [Keh and Chang (2010)], in which excellent accuracy and convergence behavior were achieved. Our solutions of the hydrodynamic drag force F exerted on the confined prolate spheroid normalized by the corresponding drag F_0 acting on an unconfined spheroid (i.e., as $b/R=0$) are presented in Tables 1 and 2 for various values of the particle aspect ratio a/b, particle slip parameter $\beta b/\eta$, wall slip parameter $\beta_w b/\eta$, and particle-wall spacing parameter b/R. The results converge to at least the significant figures as given. For the difficult case of $b/R=0.975$, the number of collocation points with $M=50$ and $N=10$ is sufficiently large to achieve this convergence. For the special cases of $a/b=1$ and $\beta b/\eta=\beta_w b/\eta \to \infty$, our results are in excellent agreement with the available solutions for the axisymmetric motions of a slip sphere in a slip circular capillary [Keh and Chang (2007)] and of a no-slip spheroid in a no-slip capillary [Yeh and Keh (2013)], respectively.

The numerical results for the normalized hydrodynamic drag force F/F_0 (or viscous retardation) for the axially symmetric migration of a prolate spheroid with aspect ratio $a/b=2$ in a circular capillary as functions of the spacing parameter b/R and particle slip parameter $\beta b/\eta$ are plotted in Fig. 2 for the limiting cases of no-slip capillary wall ($\beta_w b/\eta \to \infty$) and perfect-slip capillary wall ($\beta_w b/\eta = 0$). Analogous to the corresponding motion of a spherical particle, Tables 1 and 2 as well as Fig. 2 show that the approach of the capillary wall can significantly enhance the hydrodynamic drag experienced by the spheroid. For a spheroid with given values of a/b, $\beta b/\eta$, and $\beta_w b/\eta$, the value of F/F_0 increases monotonically with an increase in the ratio b/R from unity at $b/R=0$ to infinity in the touching limit $b/R\to 1$. The normalized wall-corrected drag force exerted on the spheroid in general decreases with decreases in $\beta b/\eta$ and $\beta_w b/\eta$ (i.e., with increasing slippage at the solid surfaces), keeping a/b and b/R unchanged. Interestingly, when the capillary wall does not slip much (with a large value of $\beta_w b/\eta$) and the value of b/R is close to unity (especially as a/b is large), F/F_0 first decreases with an increase in $\beta b/\eta$ from $\beta b/\eta=0$, reaches a minimum at some finite value of $\beta b/\eta$, and then increases with increasing $\beta b/\eta$ to the limit $\beta b/\eta\to\infty$.

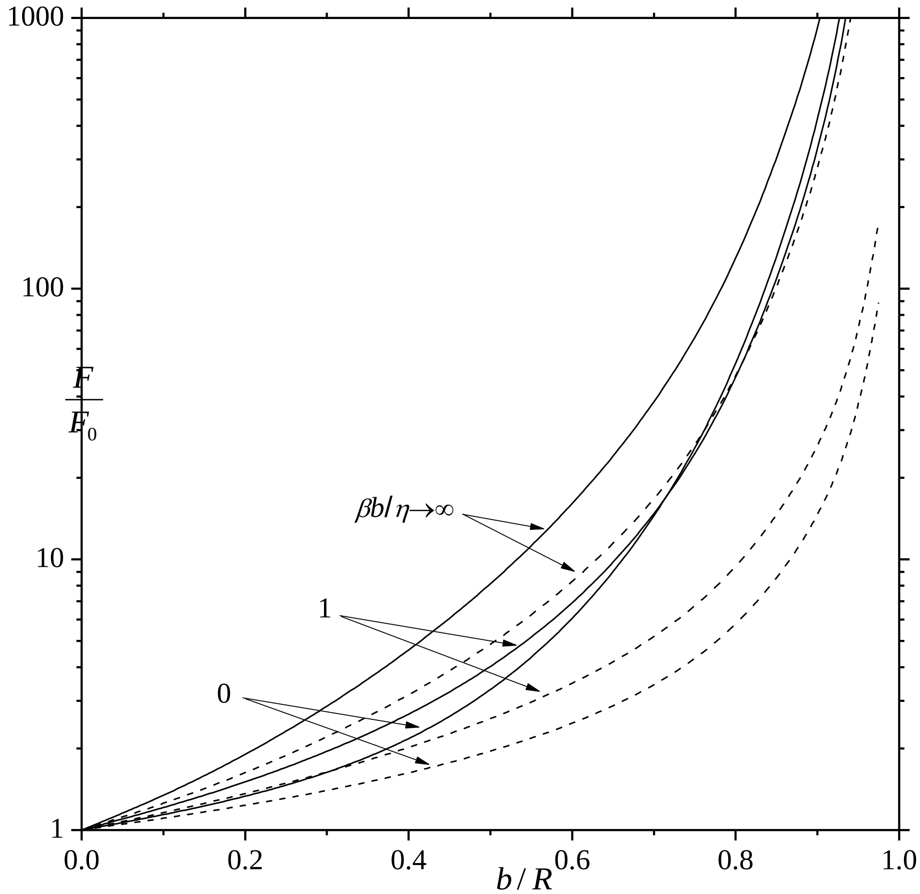

Figure 2a: Plots of the normalized drag force F/F_0 for the axially symmetric migration of a prolate spheroid with $a/b=2$ in a circular capillary for various values of the spacing parameter b/R and particle slip parameter $\beta b/\eta$: (a) F/F_0 versus b/R ; (b) F/F_0 versus $\beta b/\eta$. The solid and dashed curves represent the cases of $\beta_w b/\eta \rightarrow \infty$ and $\beta_w b/\eta = 0$, respectively.

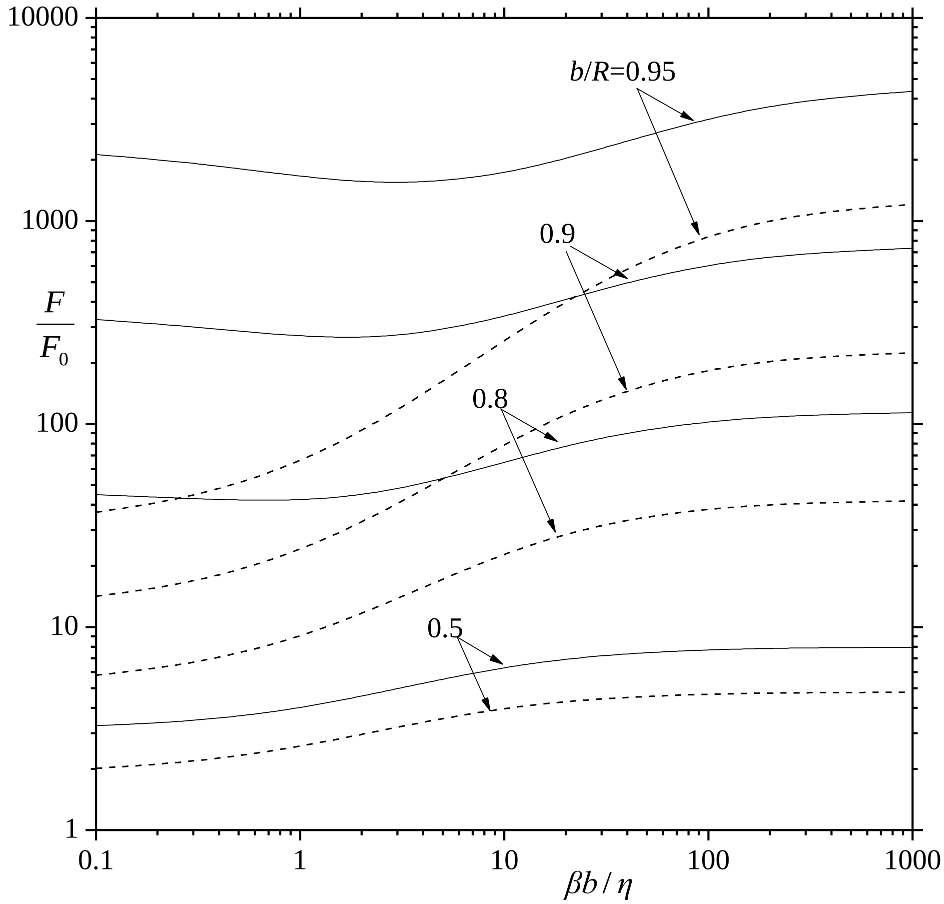

Figure 2b: Plots of the normalized drag force F/F_0 for the axially symmetric migration of a prolate spheroid with $a/b=2$ in a circular capillary for various values of the spacing parameter b/R and particle slip parameter $\beta b/\eta$: (a) F/F_0 versus b/R; (b) F/F_0 versus $\beta b/\eta$. The solid and dashed curves represent the cases of $\beta_{\mathrm{w}} b/\eta \to \infty$ and $\beta_{\mathrm{w}} b/\eta = 0$, respectively.

In Fig. 3, the results of the normalized drag force F/F_0 for the axially symmetric migration of a prolate spheroid with $\beta b/\eta \to \infty$ and $\beta b/\eta = 0$ in a circular capillary with $\beta_{\mathrm{w}} b/\eta = 0$ are plotted versus $(a/b)^{-1}$ for various values of b/R. Tables 1 and 2 as well as Fig. 3 indicate that, for given values of b/R, $\beta b/\eta$, and $\beta_{\mathrm{w}} b/\eta$, the ratio F/F_0 in general is an increasing function of a/b, since the increase in the surface area of the spheroid for its viscous interaction with the capillary wall enhances the hydrodynamic resistance to the motion of the particle. However, when $\beta b/\eta \to 0$ and either $\beta_w b/\eta$ or b/R is small, F/F_0 decreases with an increase in a/b (and a minimum of F/F_0 can appear at some intermediate value of a/b as $\beta_w b/\eta$ is large), due to the slippage at the particle surface. In general, F/F_0 is not a very sensitive function of a/b in the range of $1 \le a/b \le 5$.

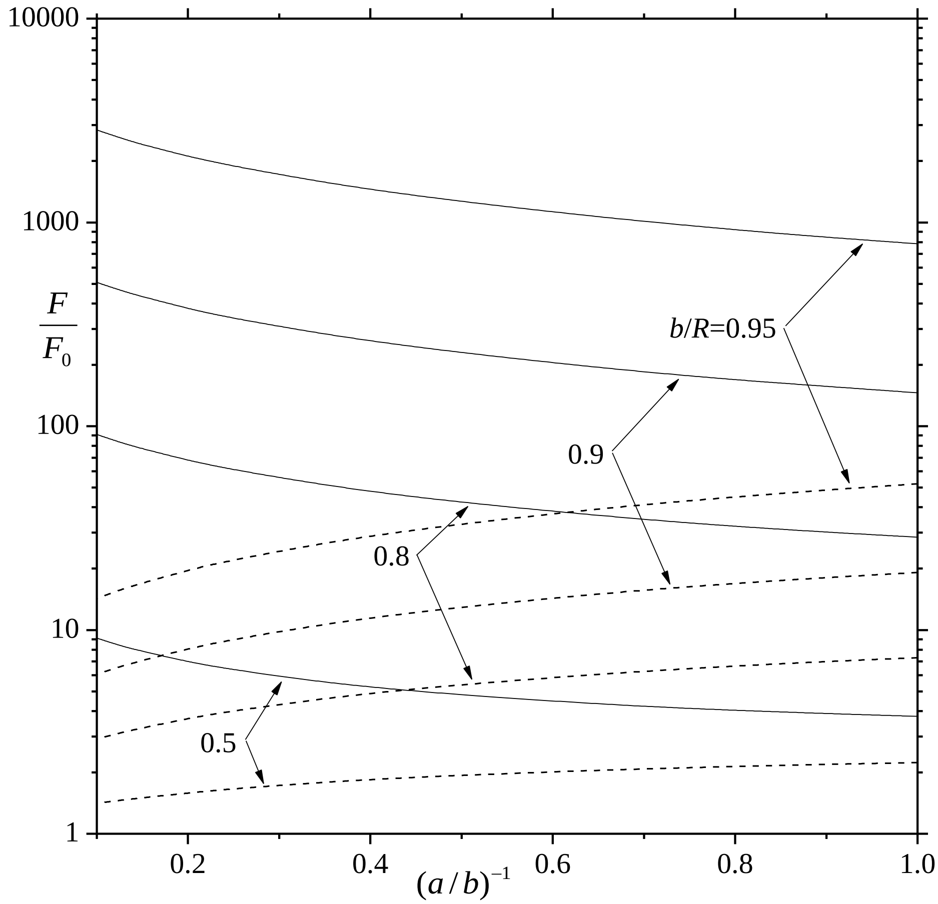

Figure 3: Plots of the normalized drag force F/F_0 for the axially symmetric migration of a prolate spheroid in a circular capillary with $\beta_w b/\eta = 0$ versus the reciprocal of particle aspect ratio $(a/b)^{-1}$ for various values of the spacing parameter b/R. The solid and dashed curves represent the cases of $\beta b/\eta \to \infty$ and $\beta b/\eta = 0$, respectively.

Table 1: The normalized drag force F/F_0 exerted on a prolate spheroid migrating axi-symmetrically in a circular capillary with $\beta_w b/\eta \to \infty$ at various values of the parameters a/b, b/R, and $\beta b/\eta$

	b/R	F/F_0				
		$a/b=1$	$a/b=1.1$	$a/b=2$	$a/b=5$	$a/b=10$
$\beta b/\eta=0$	0.2	1.38994	1.38112	1.32266	1.23619	1.22659
	0.4	2.26263	2.23987	2.13082	2.35959	3.62265
	0.6	5.20429	5.21679	5.81098	11.1320	26.6718
	0.8	28.5678	29.9408	46.5531	136.996	377.029
	0.9	173.333	187.679	344.821	1132.97	3186.70
	0.95	1038.85	1145	2262	7703	2.179E4
	0.975	6079.21	6.75E3	1.4E4	4.8E4	1.3E5
$\beta b/\eta=1$	0.2	1.45243	1.45406	1.49771	1.70718	1.97130
	0.4	2.48508	2.49384	2.64515	3.19896	3.80162
	0.6	5.82728	5.89792	6.68534	8.86535	10.8925
	0.8	29.9541	31.1132	41.3588	63.3509	80.7207
	0.9	168.989	179.649	267.260	438.547	566.12
	0.95	968.946	1045.2	1651	2.79E3	3.62E3
	0.975	5537.71	6.0E3	9.8E3	1.7E4	2.2E4
$\beta b/\eta=10$	0.2	1.60234	1.61928	1.78145	2.26487	2.80363
	0.4	3.15199	3.22945	3.91968	5.62315	7.26154
	0.6	8.47578	8.80325	11.5369	17.6430	23.1767
	0.8	44.2658	46.5644	64.8637	103.224	136.795
	0.9	218.182	231.255	332.742	538.696	716.06
	0.95	1068.52	1139.13	1677	2742	3.65E3
	0.975	5392.05	5.78E3	8.6E3	1.4E4	1.9E4
$\beta b/\eta\to\infty$	0.2	1.67948	1.69931	1.88312	2.42095	3.02003
	0.4	3.59137	3.69166	4.55952	6.67121	8.70883
	0.6	11.0919	11.5882	15.6331	24.5529	32.6570
	0.8	74.6688	79.2303	114.777	188.254	252.677

	0.9	469.170	501.699	749.832	1248.51	1679.50
	0.95	2806.65	3013.32	4569.68	7644.97	10264.2
	0.975	16290.8	1.756E4	2.668E4	4.431E4	5.85E4

Table 2: The normalized drag force F/F_0 exerted on a prolate spheroid migrating axisymmetrically in a circular capillary with $\beta_w = \beta$ at various values of the parameters a/b, b/R, and $\beta b/\eta$.

	b/R	F/F_0				
		$a/b=1$	$a/b=1.1$	$a/b=2$	$a/b=5$	$a/b=10$
$\beta b/\eta=0$	0.2	1.28429	1.27753	1.23090	1.14858	1.09530
	0.4	1.79341	1.77058	1.61689	1.38638	1.26303
	0.6	2.94404	2.87596	2.44676	1.90213	1.63662
	0.8	7.30773	7.02413	5.40400	3.67536	2.91480
	0.9	19.1777	18.1979	12.9976	8.07134	6.05778
	0.95	52.0427	48.9315	33.2759	19.5993	14.2682
	0.975	143.951	135	88.8	50.9	36.5
$\beta b/\eta=1$	0.2	1.39014	1.39142	1.42827	1.61249	1.85204
	0.4	2.10471	2.10813	2.20026	2.59535	3.05298
	0.6	3.81055	3.81697	4.02586	4.91454	5.88804
	0.8	10.7322	10.7490	11.5805	14.9830	18.3855
	0.9	30.5543	30.6067	33.7131	45.6005	56.7584
	0.95	87.0755	87.2365	97.7186	135.913	170.460
	0.975	247.685	248.14	281.04	397	500
$\beta b/\eta=10$	0.2	1.58608	1.60248	1.75956	2.22981	2.75641
	0.4	2.99068	3.06122	3.69285	5.26618	6.78857
	0.6	7.25645	7.52223	9.75909	14.8142	19.4261
	0.8	29.4427	30.8675	42.3615	66.8508	88.4499
	0.9	104.116	109.751	154.475	247.5	328
	0.95	335.569	354.785	506.12	816.9	1.1E3
	0.975	1022.01	1082.4	1.55E3	2.5E3	3.4E3

4 Motion of a prolate Cassini oval

The method of combined singularity distribution and boundary collocation is used in this section to solve for the hydrodynamic drag force experienced by a prolate Cassini oval undergoing axial symmetric migration in a circular capillary with slip surfaces. The surface of a prolate Cassini oval [Keh and Tseng (1994)] and the local components of its outward unit normal in cylindrical coordinates are expressed by

$$\rho = [(4c^2z^2 + d^4)^{1/2} - z^2 - c^2]^{1/2}, \tag{19}$$

and

$$n_\rho = \frac{\rho}{\sqrt{\rho^2 + v^2z^2}}, \qquad n_z = \frac{vz}{\sqrt{\rho^2 + v^2z^2}}, \tag{20}$$

where $0 \le c \le d$, $|z| \le (d^2 + c^2)^{1/2}$, and $v = 1 - 2c^2(4c^2z^2 + d^4)^{-1/2}$. If the shape parameter $(c/d)^2 \le 1/2$, the surface of the Cassini oval is convex everywhere, and its maximal radius of transverse circle develops at $z = 0$ and equals $(d^2 - c^2)^{1/2}$; the particle degenerates to a sphere of radius d in the limit $c = 0$. If $1/2 < (c/d)^2 \le 1$, the surface of the Cassini oval is concave at $z = 0$, and its maximal radius of transverse circle occurs at $|z| = c(1 - d^4/4c^4)^{1/2}$ (or $v = 0$) and equals $d^2/2c$.

In Tables 3 and 4, numerical results of the drag force F exerted by the fluid on a prolate Cassini oval migrating axi-symmetrically in a circular capillary normalized by its value F_0 in an unbounded fluid (i.e., as $b/R = 0$) are presented for various values of the slip parameters $\beta b/\eta$ and $\beta_w b/\eta$, particle shape parameter $(c/d)^2$ (up to 0.95), and particle-wall spacing parameter b/R (up to 0.975), where b is the larger one between $(d^2 - c^2)^{1/2}$ and $d^2/2c$ now. Again, our solutions for the limiting cases of $(c/d)^2 = 0$ (same as those given for the case of $a/b = 1$ in Tables 1 and 2) and $\beta b/\eta = \beta_w b/\eta \to \infty$ agree excellently with the results for the axisymmetric motions of a slip sphere in a slip circular capillary [Keh and Chang (2007)] and of a no-slip Cassini oval in a no-slip capillary [Yeh and Keh (2013)], respectively.

Numerical values of the normalized hydrodynamic drag force F/F_0 for the axially symmetric migration of a prolate Cassini oval with shape parameter $(c/d)^2 = 0.8$ in a circular capillary as a function of the spacing parameter b/R and particle slip parameter $\beta b/\eta$ are plotted in Fig. 4 for the cases of no-slip capillary wall ($\beta_w b/\eta \to \infty$) and perfect-slip capillary wall ($\beta_w b/\eta = 0$). Similar to the corresponding motion of a slip prolate spheroid considered in the previous section, Tables 3 and 4 as well as Fig.4 also show that the approach of the capillary wall can substantially increase the hydrodynamic drag experienced by the slip Cassini oval. For a Cassini oval with a given shape parameter $(c/d)^2$, the value of F/F_0 increases monotonically with an increase in the ratio b/R from unity at $b/R=0$ to infinity in the touching limit $b/R=1$, and in general decreases with decreases in $\beta b/\eta$ and $\beta_w b/\eta$. Again, when the capillary wall does not slip much and the value of b/R is close to unity, F/F_0 first decreases with an increase in $\beta b/\eta$ from $\beta b/\eta=0$ before attaining a minimum, and then increases with a further increase in $\beta b/\eta$.

Table 3: The normalized drag force F/F_0 exerted on a prolate Cassini oval migrating axisymmetrically in a circular capillary with $\beta_w b/\eta \to \infty$ at various values of the parameters $(c/d)^2$, b/R, and $\beta b/\eta$.

	b/R	F/F_0					
		$(c/d)^2=0.1$	0.3	0.5	0.7	0.9	0.95
$\beta b/\eta=0$	0.2	1.38107	1.36811	1.37466	1.39893	1.47766	1.52215
	0.4	2.24025	2.21788	2.27906	2.35137	2.46267	2.55364
	0.6	5.22562	5.43223	6.25973	6.87448	6.53663	6.48663
	0.8	30.1347	35.8549	52.6455	58.7969	45.9694	42.9173
	0.9	189.655	247.132	435.234	437.424	309.436	283.4
	0.95	1159.6	1589.2	3278	2799	1927	1756
	0.975	6.86E3	9.66E3	2.33E4	1.66E4	1.2E4	1.0E4
$\beta b/\eta=1$	0.2	1.45195	1.45979	1.49462	1.54145	1.60159	1.62832
	0.4	2.48621	2.52046	2.65659	2.77281	2.83221	2.88527
	0.6	5.88098	6.14732	7.00415	7.53237	7.16371	7.12980
	0.8	31.2095	35.7861	49.5806	53.8195	44.2368	42.4105
	0.9	181.396	225.185	373.703	368.612	278.600	263.570
	0.95	1060.07	1384.02	2704.70	2276.95	1683.345	1587.0
	0.975	6.12E3	8.23E3	1.89E4	1.33E4	9.8E3	9.3E3
$\beta b/\eta=10$	0.2	1.61821	1.66735	1.76277	1.86421	1.90996	1.91586
	0.4	3.22276	3.43993	3.86793	4.21738	4.14653	4.10128
	0.6	8.76464	9.66079	11.5841	12.6343	11.3863	11.0555
	0.8	46.2737	52.9330	70.8405	74.2589	59.5853	57.1358
	0.9	230.340	273.363	419.725	400.932	304.527	291.893
	0.95	1140.52	1405.27	2535.2	2093.5	1583.1	1521.0
	0.975	5.80E3	7.39E3	1.58E4	1.1E4	8.5E3	8.2E3

$\beta b/\eta \to \infty$	0.2	1.70173	1.76840	1.89405	2.03118	2.09774	2.10648
	0.4	3.70451	4.04497	4.71003	5.31421	5.29098	5.23439
	0.6	11.6571	13.3944	17.1162	19.6686	17.8918	17.3608
	0.8	79.9433	97.0826	141.978	155.944	125.345	120.368
	0.9	507.226	637.551	1063.90	1037.97	790.890	759.547
	0.95	3050.36	3919.74	7511.60	6214.28	4723.97	4522.7
	0.975	17748.3	23094.7	50904.0	35308.8	27262	2.6E4

Table 4: The normalized drag force F/F_0 exerted on a prolate Cassini oval migrating axi-symmetrically in a circular capillary with $\beta_w = \beta$ at various values of the parameters $(c/d)^2$, b/R, and $\beta b/\eta$.

	b/R	F/F_0					
		$(c/d)^2 = 0.1$	0.3	0.5	0.7	0.9	0.95
$\beta b/\eta = 0$	0.2	1.27745	1.26675	1.26937	1.28727	1.35041	1.38371
	0.4	1.77000	1.72988	1.72339	1.74568	1.88244	1.96697
	0.6	2.87268	2.73975	2.70044	2.77908	3.10535	3.24268
	0.8	6.99948	6.37005	6.17658	6.98081	8.29713	8.4161
	0.9	18.0791	15.646	14.748	19.469	23.306	22.989
	0.95	48.4717	39.971	35.904	57.46	65.87	63.85
	0.975	132.9	105.3	88.0	1.7E2	1.9E2	-
$\beta b/\eta = 1$	0.2	1.38800	1.39043	1.41355	1.44730	1.49549	1.51687
	0.4	2.09603	2.09673	2.15549	2.21298	2.28235	2.33043
	0.6	3.77979	3.76223	3.92313	4.02713	4.06824	4.13071
	0.8	10.5899	10.4875	11.4597	11.9230	11.5656	11.4850
	0.9	30.0529	29.7236	34.7742	36.1288	33.4735	32.6472
	0.95	85.4745	84.4997	107.542	108.088	96.2755	92.92
	0.975	242.820	239.929	336.931	316.822	274.9	264
$\beta b/\eta = 10$	0.2	1.60063	1.64586	1.73371	1.82601	1.86665	1.87178
	0.4	3.04809	3.22551	3.57482	3.84983	3.77921	3.73898
	0.6	7.44631	8.04222	9.31638	9.92034	8.95006	8.69091
	0.8	30.2752	33.1420	40.9494	41.3566	33.1167	31.6255
	0.9	106.971	118.082	157.899	146.248	108.841	103.346

0.95	344.508	383.401	566.270	464.278	334.720	317.3
0.975	1.05E3	1176	1954.78	1383.1	991	9.4E2

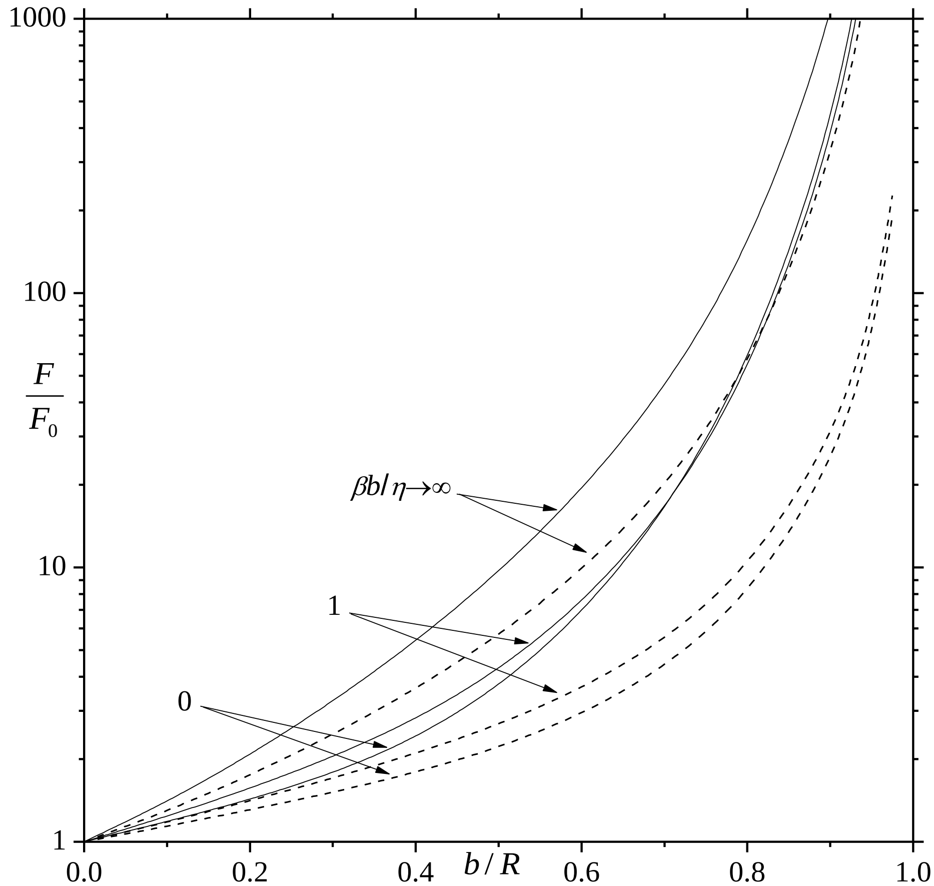

Figure 4a: Plots of the normalized drag force F/F_0 for the axially symmetric migration of a prolate Cassini oval with $(c/d)^2 = 0.8$ in a circular capillary for various values of the spacing parameter b/R and particle slip parameter $\beta b/\eta$: (a) F/F_0 versus b/R; (b) F/F_0 versus $\beta b/\eta$. The solid and dashed curves represent the cases of $\beta_w b/\eta \to \infty$ and $\beta_w b/\eta = 0$, respectively.

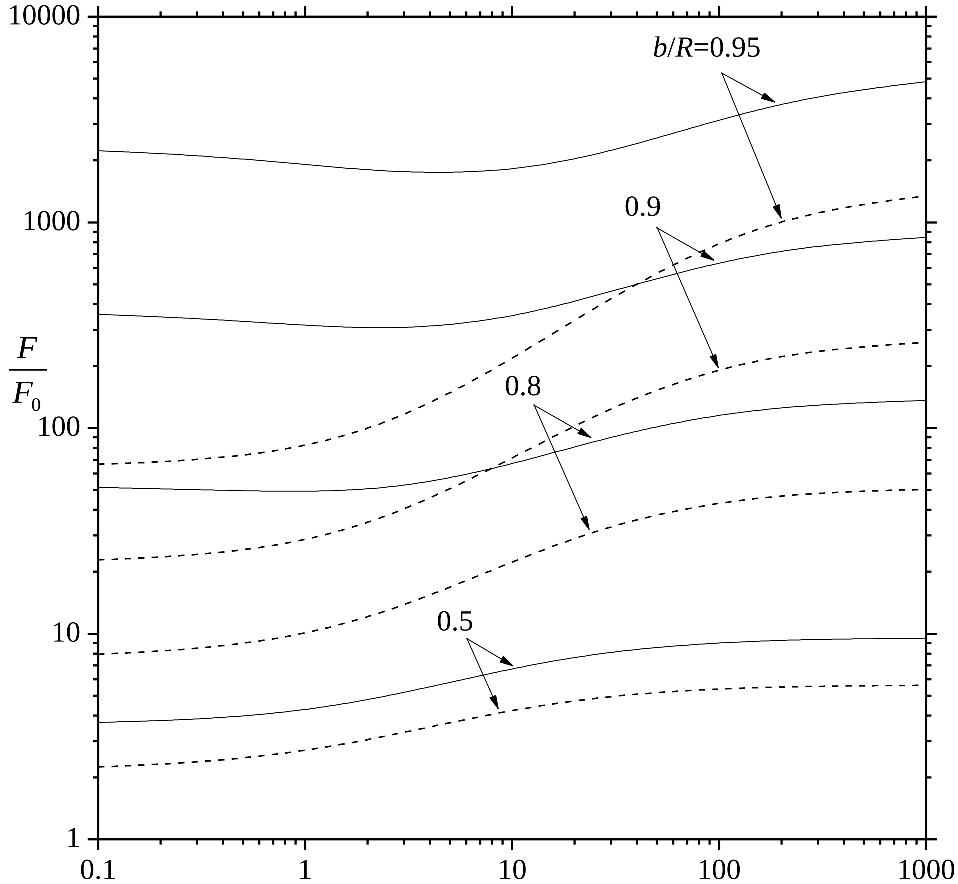

Figure 4b: Plots of the normalized drag force F/F_0 for the axially symmetric migration of a prolate Cassini oval with $(c/d)^2 = 0.8$ in a circular capillary for various values of the spacing parameter b/R and particle slip parameter $\beta b/\eta$: (a) F/F_0 versus b/R; (b) F/F_0 versus $\beta b/\eta$. The solid and dashed curves represent the cases of $\beta_w b/\eta \to \infty$ and $\beta_w b/\eta = 0$, respectively.

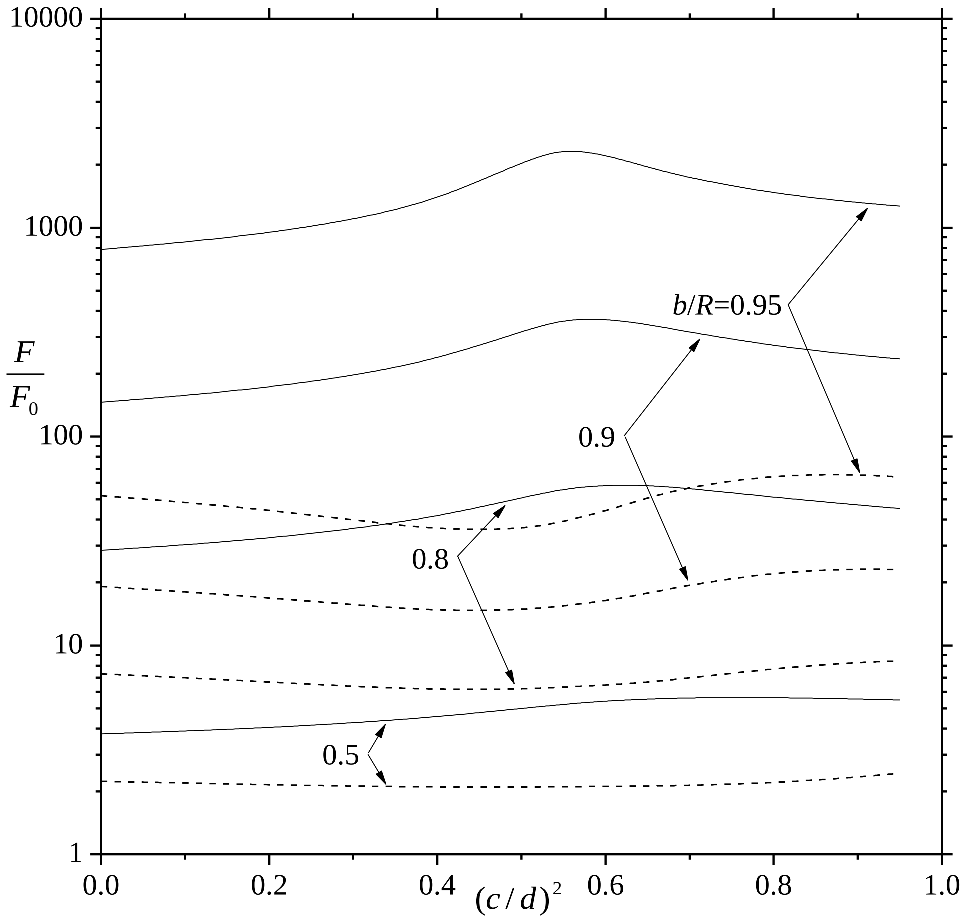

Figure 5: Plots of the normalized drag force F/F_0 for the axially symmetric migration of a prolate Cassini oval in a circular capillary with $\beta_w b/\eta = 0$ versus the particle shape parameter $(c/d)^2$ for various values of the spacing parameter b/R. The solid and dashed curves represent the cases of $\beta b/\eta \to \infty$ and $\beta b/\eta = 0$, respectively.

In Fig. 5, the results of the normalized drag force F/F_0 for the axially symmetric migration of a prolate Cassini oval with $\beta b/\eta \to \infty$ and $\beta b/\eta = 0$ in a circular capillary with $\beta_w b/\eta = 0$ as a function of its shape parameter $(c/d)^2$ for various values of the spacing parameter b/R are plotted. Tables 3 and 4 as well as Fig. 5 indicate that, for a given value of b/R and a relatively large value of $\beta b/\eta$ or $\beta_w b/\eta$, the ratio F/F_0 in general increases with an increase in $(c/d)^2$ in the range of $0 \le (c/d)^2 \le 1/2$ (due to the increase in the surface area of the Cassini oval for its viscous interaction with the capillary wall), but can reach a maximum at a value of

$(c/d)^2 > 1/2$ (this value increases with decreasing b/R) and then decrease with a further increase in $(c/d)^2$ (because the increase in the concave portion of the Cassini oval reduces the hydrodynamic retardation effect of the capillary wall). However, when $\beta b/\eta \to 0$ and either $\beta_{\mathrm{w}} b/\eta$ or b/R is small, F/F_0 can first decrease with an increase in $(c/d)^2$, reach a minimum at some value of $(c/d)^2$, and then increase with a further increase in $(c/d)^2$, due to the slippage at the particle surface. For the case of large b/R and small to moderate $\beta b/\eta$ and $\beta_{\mathrm{w}} b/\eta$, F/F_0 can encounter both a minimum and a maximum with an increase in $(c/d)^2$ in the whole range. Also, F/F_0 is not a very sensitive function of $(c/d)^2$ in the whole range, but the boundary effect on the migration of the particle is significant.

5 Conclusions

The creeping motion of an axisymmetric prolate particle along its axis of revolution in a coaxial circular capillary with slip-flow surfaces is examined by using the method of combined singularity distribution and boundary collocation. The convergent and accurate solutions of the normalized hydrodynamic drag force F/F_0 for the axially symmetric migrations of a prolate spheroid and of a prolate Cassini oval are obtained for broad ranges of the particle aspect ratio a/b and shape parameter $(c/d)^2$, respectively, the particle-wall separation parameter b/R, the particle slip parameter $\beta b/\eta$, and the wall slip parameter $\beta_{\mathrm{w}} b/\eta$. For constant values of b/R and a/b or $(c/d)^2$, the normalized drag F/F_0 in general decreases with decreasing $\beta b/\eta$ and $\beta_{\mathrm{w}} b/\eta$ (increasing slippage at the solid surfaces), but there are exceptions when the values of both $\beta_{\mathrm{w}} b/\eta$ and b/R are large. For given values of b/R, $\beta b/\eta$, and $\beta_{\mathrm{w}} b/\eta$, the normalized drag F/F_0 increases with an increase in the axial-to-radial aspect ratio of the particle (or effective surface area for the particle-wall hydrodynamic interaction), but this trend can be reversed as $\beta b/\eta$ is small (the particle is highly slippery). The boundary effect of the capillary wall on the migration of the particle is significant when they are close to each other.

Appendix A: Definitions of functions in Section 2. Some functions in Section 2 are defined as

$$A_{in}(\rho,z,h) = \int_0^\infty [S_{in}^{(1)}(\omega,z,h)\omega\rho I_0(\omega\rho) + S_{in}^{(2)}(\omega,z,h) I_1(\omega\rho)]\sin(\omega z)\mathrm{d}\omega$$

$$-\rho^{-1} r_h^{-n+2i-2}[(n+1)\, G_{n+1}^{-1/2}(\kappa) - 2(i-1)\kappa G_{n+1}^{-1/2}(\kappa)], \qquad \text{(A1)}$$

$$C_{in}(\rho,z,h)=\int_0^\infty\{S_{in}^{(1)}(\omega,z,h)[2I_0(\omega\rho)+\omega\rho I_1(\omega\rho)]+S_{in}^{(2)}(\omega,z,h)I_0(\omega\rho)\}\cos(\omega z)\mathrm{d}\omega$$
$$-r_h^{-n+2i-3}[P_n(\kappa)+2(i-1)G_n^{-1/2}(\kappa)], \qquad \text{(A2)}$$

$$\alpha_{in}(\rho,z,h)=2\int_0^\infty\{S_{in}^{(1)}(\omega,z,h)[I_0(\omega\rho)+\omega\rho I_1(\omega\rho)]$$
$$+S_{in}^{(2)}(\omega,z,h)[I_0(\omega\rho)-(\omega\rho)^{-1}I_1(\omega\rho)]\}\sin(\omega z)\omega\mathrm{d}\omega$$
$$+2\rho^{-2}r_h^{-n+2i-4}\{(n+1)[(n-2i+2)\rho^2+r_h^2]G_{n+1}^{-1/2}(\kappa)-(n+1)\rho^2\kappa P_n(\kappa)$$
$$-2(i-1)[(n-2i+3)\rho^2+r_h{}^2]\kappa G_n^{-1/2}(\kappa)+2(i-1)\rho^2\kappa^2P_{n-1}(\kappa)\}, \qquad \text{(A3)}$$

$$\beta_{in}(\rho,z,h)=2\int_0^\infty\{S_{in}^{(3)}(\omega,z,h)[2I_0(\omega\rho)+\omega\rho I_1(\omega\rho)]+S_{in}^{(4)}(\omega,z,h)I_0(\omega\rho)\}\omega\mathrm{d}\omega$$
$$+2r_h^{-n+2i-4}\{(2n-2i+3)\kappa P_n(\kappa)-nP_{n-1}(\kappa)$$
$$+2(i-1)[(n-2i+3)\kappa G_n^{-1/2}(\kappa)+(1-\kappa^2)P_{n-1}(\kappa)]\}, \qquad \text{(A4)}$$

$$\gamma_{in}(\rho,z,h)=\int_0^\infty\{S_{in}^{(1)}(\omega,z,h)[\omega\rho I_0(\omega\rho)+2I_1(\omega\rho)]+S_{in}^{(2)}(\omega,z,h)I_1(\omega\rho)\}\cos(\omega z)\omega\mathrm{d}\omega$$
$$+\int_0^\infty[S_{in}^{(5)}(\omega,z,h)\omega\rho I_0(\omega\rho)+S_{in}^{(6)}(\omega,z,h)I_1(\omega\rho)]\omega\mathrm{d}\omega$$
$$+\rho^{-1}r_h^{-n+2i-5}\{(n+1)(n-2i+2)r_h{}^2\kappa G_{n+1}^{-1/2}(\kappa)$$
$$+[2(n-i+2)\rho^2-nz_h{}^2]P_n(\kappa)+nr_h{}^2\kappa P_{n-1}(\kappa)$$
$$+2(i-1)[(n-2i+3)(\rho^2-z_h{}^2)+r_h{}^2]G_n^{-1/2}(\kappa)-4(i-1)\rho^2\kappa P_{n-1}(\kappa)]\}, \qquad \text{(A5)}$$

where $i=1$ and 2;

$$S_{in}^{(1)}(\omega,z,h)=H_2(\omega)[W_{in}^{(1)}(\omega,z,h)H_1(\omega)-W_{in}^{(2)}(\omega,z,h)I_1(\omega R)], \qquad \text{(A6)}$$

$$S_{in}^{(2)}(\omega,z,h)=\frac{1}{I_1(\omega R)}[W_{in}^{(1)}(\omega,z,h)-\omega RI_0(\omega R)S_{in}^{(1)}(\omega,z,h)], \qquad \text{(A7)}$$

$$S_{in}^{(3)}(\omega,z,h)=H_2(\omega)[W_{in}^{(1)}(\omega,z,0)\Omega_1(\omega,z,h)H_1(\omega)+W_{in}^{(2)}(\omega,z,0)\sin(\omega z_h)I_1(\omega R)], \qquad \text{(A8)}$$

$$S_{in}^{(4)}(\omega,z,h)=\frac{1}{I_1(\omega R)}[W_{in}^{(1)}(\omega,z,0)\Omega_1(\omega,z,h)-\omega RI_0(\omega R)S_{in}^{(3)}(\omega,z,h)] \qquad \text{(A9)}$$

$$S_{in}^{(5)}(\omega,z,h)=H_2(\omega)[W_{in}^{(1)}(\omega,z,0)\cos(\omega z_h)H_1(\omega)-W_{in}^{(2)}(\omega,z,0)\Omega_2(\omega,z,h)I_1(\omega R)], \qquad \text{(A10)}$$

$$S_{in}^{(6)}(\omega,z,h)=\frac{1}{I_1(\omega R)}[W_{in}^{(1)}(\omega,z,0)\cos(\omega z_h)-\omega R I_0(\omega R) S_{in}^{(5)}(\omega,z,h)] \quad ; \qquad \text{(A11)}$$

$$W_{1n}^{(1)}(\omega,z,h)=-(-1)^{n/2}\frac{2\omega^n}{\pi n!}K_1(\omega R)\frac{\sin(\omega z_h)}{\sin(\omega z)} , \qquad \text{(A12)}$$

$$W_{2n}^{(1)}(\omega,z,h)=(-1)^{n/2}\frac{2\omega^{n-2}}{\pi n!}[(n-2)(n-3)K_1(\omega R)-(2n-3)\omega R K_0(\omega R)]\frac{\sin(\omega z_h)}{\sin(\omega z)}$$
(A13)

$$W_{1n}^{(2)}(\omega,z,h)=(-1)^{n/2}\frac{2\omega^n}{\pi n!}[K_0(\omega R)-\frac{2\eta}{\beta_{\mathrm{w}}}\omega K_1(\omega R)]\frac{\cos(\omega z_h)}{\cos(\omega z)} , \qquad \text{(A14)}$$

$$W_{2n}^{(2)}(\omega,z,h)=(-1)^{n/2}\frac{2\omega^{n-2}}{\pi n!}\{[(2n-3)\omega R+\frac{2\eta}{\beta_{\mathrm{w}}}\omega(n^2-3n+3)]K_1(\omega R)$$

$$-[n(n-1)+\frac{2\eta}{\beta_{\mathrm{w}}}\omega^2 R(2n-3)]K_0(\omega R)\}\frac{\cos(\omega z_h)}{\cos(\omega z)} ; \qquad \text{(A15)}$$

$$H_1(\omega)=I_0(\omega R)+\frac{2\eta}{\beta_{\mathrm{w}}}\omega I_1(\omega R) , \qquad \text{(A16)}$$

$$H_2(\omega)=[\omega R I_0{}^2(\omega R)-2I_0(\omega R)I_1(\omega R)-(R+\frac{2\eta}{\beta_{\mathrm{w}}})\omega I_1{}^2(\omega R)]^{-1} \quad ; \qquad \text{(A17)}$$

$$\Omega_1(\omega,z,h)=\cos(\omega z_h)\cot(\omega z)-\sin(\omega z_h)\csc^2(\omega z) , \qquad \text{(A18)}$$

$$\Omega_2(\omega,z,h)=\cos(\omega z_h)\sec^2(\omega z)-\sin(\omega z_h)\tan(\omega z) ; \qquad \text{(A19)}$$

$$r_h=(\rho^2+z_h^2)^{1/2} , \qquad z_h=z-h , \qquad \kappa=z_h/r_h ; \qquad \text{(A20)}$$

I_m and K_m are the modified Bessel functions of the first and second kinds, respectively, of order m; $G_n^{-1/2}$ is the Gegenbauer polynomial of the first kind of order n and degree –1/2; P_n is the Legendre polynomial of order n.

References

Basset, A. B. (1961): *A treatise on hydrodynamics*, vol. *2*, Dover, New York.

Batchelor, G. K. (1970): Slender-body theory for particles of arbitrary cross-section in Stokes flow. *J. Fluid Mech.*, vol. 44, pp. 419-440.

Brenner, H. (1964): The Stokes resistance of a slightly deformed sphere. *Chem. Eng. Sci.*, 19, 519-539.

Chang, Y. C.; Keh, H. J. (2006): Slow motion of a slip spherical particle perpendicular to two plane walls. *J. Fluids Structures*, vol.22, pp.647-661.

Chang, Y. C.; Keh, H. J. (2009): Translation and rotation of slightly deformed colloidal spheres experiencing slip. *J. Colloid Interface Sci.*, vol.330, no.1, 201-210.

Chang, Y. C.; Keh, H. J. (2011): Theoretical study of the creeping motion of axially and fore-and-aft symmetric slip particles in an arbitrary direction. *Eur. J. Mech. B Fluids*, vol.30, pp.236-244.

Chen, P. Y.; Keh, H. J. (2003): Slow motion of a slip spherical particle parallel to one or two plane walls. *J. Chin. Inst. Chem. Engrs.*, vol.34, pp.123-133.

Chen, S. H.; Keh, H. J. (1995): Axisymmetric motion of two spherical particles with slip surfaces. *J. Colloid Interface Sci.*, vol.171, pp.63-72.

Chiu, H. C.; Keh, H. J. (2016): Electrophoresis of a colloidal sphere with double layer polarization in a microtube. *Microfluid. Nanofluid., vol.* 20, no.64-1-13.

Chiu, H. C.; Keh, H. J. (2017): Diffusiophoresis of a charged particle in a microtube. *Electrophoresis*, vol.38, pp. 2468-2478.

Churaev, N. V.; Sobolev, V. D.; Somov, A. N. (1984): Slippage of liquids over lyophobic solid surfaces. *J. Colloid Interface Sci.*, vol.97, pp.574-581.

Chwang, A. T.; Wu, T. Y. (1975): Hydrodynamic of low-Reynolds-number flow, Part 2. Singularity method for Stokes flows. *J. Fluid Mech.*, vol.67, pp.787-815.

Dassios, G.; Hadjinicolaou, M.; Payatakes, A.C. (1994): Generalized eigenfunctions and complete semiseparable solutions for Stokes flow in spheroidal coordinates. *Quart. Appl. Math.*, vol.52, pp.157-191.

Deo, S.; Datta, S. (2002): Slip flow past a prolate spheroid. *Indian J. Pure Appl. Math.* , vol.33, pp.903-909.

Faltas, M. S.; Saad, E. I. (2011): Stokes flow past an assemblage of slip eccentric spherical particle-in-cell models. *Math. Meth. Appl. Sci.*, vol.34, pp.1594-1605.

Felderhof, B. U. (1977): Hydrodynamic interaction between two spheres. *Physica*, vol.*89A*, pp.373-384.

Gluckman, M. J.; Pfeffer, R.; Weinbaum, S. (1971): A new technique for treating multi-particle slow viscous flow: axisymmetric flow past spheres and spheroids. *J. Fluid Mech.*, vol.50, pp.705-740.

Gogte, S.; Vorobieff, P.; Truesdell, R.; Mammoli, A.; van Swol, F.; Shah, P.; Brinker, C. J. (2005): Effective slip on textured superhydrophobic surfaces. *Phys. Fluids*, vol.17, no.051701, pp.1-4.

Happel, J.; Brenner, H. (1983): *Low Reynolds number hydrodynamics.* Nijhoff, The Netherlands.

Hornbeck, R. W. (1975): *Numerical Methods*. Quantum Publishers, New York.

Hu, C. M.; Zwanzig, R. (1974): Rotational friction coefficients for spheroids with the slipping boundary condition. *J. Chem. Phys.*, vol. 60, pp.4354-4357.

Keh, H. J.; Chang, J. H. (1998): Boundary effects on the creeping-flow and thermophoretic motions of an aerosol particle in a spherical cavity. *Chem. Eng. Sci.*, vol.53, pp.2365-2377.

Keh, H. J.; Chang, Y. C. (2007): Slow motion of a slip spherical particle in a circular cylindrical pore. Int. *J. Multiphase Flow*, vol.33, pp.726-741.

Keh, H. J.; Chang, Y. C. (2008): Slow motion of a slip spheroid along its axis of revolution. *Int. J. Multiphase Flow*, vol.34, pp.713-722.

Keh, H. J.; Chang, Y. C. (2010): Slow motion of a general axisymmetric slip particle along its axis of revolution and normal to one or two plane walls. *CMES: Computer Modeling in Engineering & Sciences*, vol. 62, pp.225-253.

Keh, H. J.; Chen, S. H. (1996): The motion of a slip spherical particle in an arbitrary Stokes flow. *Eur. J. Mech., B/Fluids*, vol.15, pp.791-807.

Keh, H. J.; Huang, C. H. (2004): Slow motion of axisymmetric slip particles along their axes of revolution. *Int. J. Eng. Sci.*, vol.42, pp.1621-1644.

Keh, H. J.; Lee, T. C. (2010): Axisymmetric creeping motion of a slip spherical particle in a nonconcentric spherical cavity. *Theor. Comput. Fluid Dyn.*, vol.24, pp.497-510.

Keh, H. J.; Shiau, S. C. (2000): Effects of inertia on the slow motion of aerosol particles. *Chem. Eng. Sci.*, vol.42, pp.1621-1644.

Keh, H. J.; Tseng, C. H. (1994): Slow motion of an arbitrary axisymmetric body along its axis of revolution and normal to a plane surface. *Int. J. Multiphase Flow*, vol.20, pp.185-210.

Lee, T. C.; Keh, H. J. (2013): Slow motion of a spherical particle in a spherical cavity with slip surfaces. *Int. J. Eng. Sci.*, vol.69, pp.1-15.

Lee, T. C.; Keh, H. J. (2014): Electrophoretic motion of a charged particle in a charged cavity. *Eur. J. Mech. B/Fluids*, vol.46, pp.183-192.

Li, C. Y.; Keh, H. J. (2017): Thermophoresis of a spherical particle in a microtube. *J. Aerosol Sci.*, vol.113, pp.71-84.

Lu, S. Y.; Lee, C. T. (2002): Creeping motion of a spherical aerosol particle in a cylindrical pore. *Chem. Eng. Sci.*, vol.57, pp.1479-1484.

Martini, A.; Roxin, A.; Snurr, R. Q.; Wang, Q.; Lichter, S. (2008): Molecular mechanisms of liquid slip. *J. Fluid Mech.*, vol.600, pp.257-269.

Nir, A. (1976): Linear shear flow past a porous particle. *Appl. Sci. Res.*, vol.32, pp.313-325.

Oberbeck, A. (1876): Uber stationare Flussigkeitsbewegungen mit Berucksichtigung der inner Reibung. *J. Reine Angew. Math.*, vol.81, pp.62-80.

Palaniappan, D. (1994): Creeping flow about a slightly deformed sphere. *Z. Angew. Math. Phys.*, vol.45, pp.832-838.

Payne, L. E.; Pell, W. H. (1960): The Stokes flow problem for a class of axially symmetric bodies. *J. Fluid Mech.*, vol.7, pp.529-549.

Pit, R.; Hervet, H.; Leger, L. (2000): Direct experimental evidence of slip in hexadecane: solid interfaces. *Phys. Rev. Lett.*, vol.85, pp.980-983.

Reed, L. D.; Morrison, F. A. (1974): Particle interactions in viscous flow at small values of Knudsen number. *J. Aerosol Sci.*, vol.5, pp.175-189.

Saffman, P. G. (1971): On the boundary condition at the surface of a porous medium. *Studies Appl. Math.*, vol.50, pp.93-101.

Senchenko, S.; Keh, H. J. (2006): Slipping Stokes flow around a slightly deformed sphere. *Phys. Fluids*, vol.18, pp.088104-1-4.

Sherif, H. H.; Faltas, M. S.; Saad, E. I. (2008): Slip at the surface of a sphere translating perpendicular to a plane wall in micropolar fluid. *Z. Angew. Math. Phys.*, vol.59, pp.293-312.

Stokes, G. G. (1851): On the effect of the internal friction of fluid on pendulums. *Trans. Cambridge Phil. Soc.*, vol.9, pp.8-106.

Wan, Y. W.; Keh, H. J. (2009): Slow rotation of an axisymmetric slip particle about its axis of revolution. *CMES: Computer Modeling in Engineering & Sciences*, vol. 53, pp.73-93.

Wan, Y. W.; Keh, H. J. (2011): Slow rotation of an axially symmetric particle about its axis of revolution normal to one or two plane walls. *CMES: Computer Modeling in Engineering & Sciences*, vol. 74, pp.109-137.

Yeh, H. Y.; Keh, H. J. (2013): Axisymmetric creeping motion of a prolate particle in a cylindrical pore. *Eur. J. Mech. B Fluids*, vol.39, pp.52-58.

Ying, R.; Peters M. H. (1991): Interparticle and particle-surface gas dynamic interactions. *Aerosol Sci. Technol.*, vol.14, pp.418-433.

Youngren, G. K.; Acrivos, A. (1975): Stokes flow past a particle of arbitrary shape: a numerical method of solution. *J. Fluid Mech.*, vol.69, pp.377-403.